Available online at www.sciencedirect.com
SCIENCE DIRECT®
Journal of Catalysis 226 (2004) 88–100
JOURNAL OF CATALYSIS
www.elsevier.com/locate/jcat

Vibrational spectra of alumina- and silica-supported vanadia revisited: An experimental and theoretical model catalyst study

Norbert Magg [a], Boonchuan Immaraporn [a], Javier B. Giorgi [a,1], Thomas Schroeder [a,2], Marcus Bäumer [a,3], Jens Döbler [b], Zili Wu [c], Evgenii Kondratenko [d], Maymol Cherian [d], Manfred Baerns [d], Peter C. Stair [c], Joachim Sauer [b], Hans-Joachim Freund [a,*]

[a] *Fritz-Haber-Institut der Max-Planck-Gesellschaft, Abteilung Chemische Physik, Faradayweg 4-6, 14195 Berlin, Germany*
[b] *Humboldt-Universität zu Berlin, Institut für Chemie, Unter den Linden 6, 10099 Berlin, Germany*
[c] *Northwestern University, 633 Clark Street Evanston, IL 60208, USA*
[d] *Institute for Applied Chemistry ACA Berlin–Adlershof, PO Box 96 11 56, 12474 Berlin, Germany*

Received 9 March 2004; accepted 21 April 2004

Available online 15 June 2004

Abstract

Oxide-supported vanadia particles were prepared via evaporation of vanadium metal in an oxygen ambient. As support oxides, we have employed thin, well-ordered alumina and silica films grown on top of NiAl(110) and Mo(112) surfaces. According to our analysis, the vanadia particles exhibit very similar morphology on both supports but differ in the extent of particle–support interactions. It is shown that these differences in the vanadia–support interface region strongly affect the CO adsorption behavior of the particles. The measured vibrational spectra of the model systems are interpreted on the basis of DFT calculations for model compounds and surface models for both the vanadia/silica and the vanadia/alumina system. The combined information is then compared with Raman spectra of real catalytic materials such as vanadia supported over δ-Al_2O_3 and mesoporous SiO_2 (MCM-41) taken at different laser wavelengths. A consistent interpretation is developed, which shows that the accepted interpretation of vibrational spectra from vanadia catalysts must be revised.

Keywords: Vanadium oxide; Alumina; Silica; Scanning tunneling microscopy (STM); X-ray photoelectron spectroscopy (XPS); Infrared (IR) spectroscopy; Carbon monoxide; DFT calculation; Raman spectra; Catalysis

1. Introduction

Oxide-supported vanadia materials represent an important class of catalysts which are industrially applied in oxidation and reduction reactions [1–3]. Hence, vanadium oxides have been intensively investigated by many researchers, aiming at a deeper understanding of the correlations between structure of VO_x species and their catalytic performance. The role of the support represents a particularly interesting topic in this respect since it is well known that the choice of the support material influences the activity of vanadia catalysts by several orders of magnitude [1–3]. Empirically, it was found that the reducibility of the oxide support constitutes an important factor, in such a way that a higher reducibility is correlated with a higher activity of the whole system. V–O–support bonds, which determine the coupling between support and overlayer, have therefore been deemed the active sites in supported vanadia catalysts [2–4]. Vibrational spectroscopy has been the workhorse to arrive at those conclusions [4–9]. However, these bonds could not be directly observed in the underlying Raman studies [2–4]. Hence, their assignment was made indirectly by excluding other species, such as V=O groups and V–O–V bridges, as the active sites. Alternatively, it was proposed that the sup-

* Corresponding author. Fax: +49-30-8413-4101.
E-mail address: freund@fhi-berlin.mpg.de (H.-J. Freund).
[1] Present address: Department of Chemistry, University of Ottawa, 10 Marie Curie, Ottawa, ON, K1N 6N5, Canada.
[2] Present address: European Synchrotron Radiation Facility, 6, Rue Jules Horowitz, 38000 Grenoble, France.
[3] Present address: University Bremen, Institut für Angewandte und Physikalische Chemie, PO Box 330 440, 28334 Bremen, Germany.

0021-9517/$ – see front matter
doi:10.1016/j.jcat.2004.04.021

port has an influence only on the speciation of VO_x into V_2O_5 crystallites, monomeric and polymeric species [10]. In summary, there is still no fully consistent picture available as far as support effects are concerned.

The purpose of the present work is to provide additional insight into this topic, employing model catalyst systems with a reduced structural complexity to allow for correlations among structure, morphology, and vibrational spectra, in combination with computations of the vibrational spectra on the basis of cluster calculations. Additionally, the Raman spectra on powdered silica and alumina-supported vanadia materials, which are usually used in different vanadia-catalyzed reactions, are provided and the combined information shows the necessity to revise the traditional interpretation of vibrational spectra from supported vanadia catalysts.

Flat, well-ordered alumina and silica films have been chosen as support oxides. They can be grown in a reproducible manner and with a thickness of only a few Å on top of NiAl(110) and Mo(112) metal surfaces, respectively, thus allowing the application of a broad range of surface science techniques [11–16]. Such model systems are well suited for vibrational studies and the vibrational spectra may be directly compared with experimental results on powder real catalytic materials. In order to find a unique interpretation and a solid assignment of the spectra it is necessary to perform calculations, which are based on reasonably chosen model structures. In the present paper, we report the results of such a combination of theoretical and experimental investigations, and we show that it is necessary to revise the "generally accepted view" of vibrational spectra reported in the literature.

2. Models for DFT calculations

In order to examine monomeric and dimeric vanadia species supported on silica as shown in Fig. 1, we construct different model structures (Fig. 2) and calculate their vibrational spectra by density functional theory (DFT). The simplest model for the monomeric surface species is the $O{=}V(OSiH_3)_3$ molecule. Note that similar molecules, with larger substituents, $O{=}V[OSi(O^tBu)_3]_3$ and $O{=}V(O^iPr)_3$, have been studied experimentally [17]. However, these simple molecules have the disadvantage that the silicon atoms, unlike in silica, are not part of a ring structure and thus can move freely during the vibrational motion. We expect that this has a major influence on the vibrational spectra.

The smallest model with ring structures is derived from a polyhedral oligomeric silsesquioxane (POSS).

It can be seen as a cube with silicon atoms at the vertices of the cube and oxygen atoms at the edges. The dangling bonds of the silicon atoms are saturated with hydrogen atoms, giving a model with the composition $Si_8O_{12}H_8$. From this structure an isolated vanadium site can be constructed by replacing a Si–H moiety by V=O (model **1**, C_{3v}, see Fig. 2). This molecule is known to exist with cyclohexyl

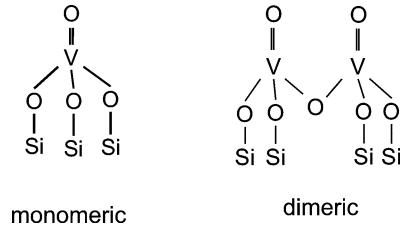

Fig. 1. Silica-supported monomeric and dimeric vanadium oxide species.

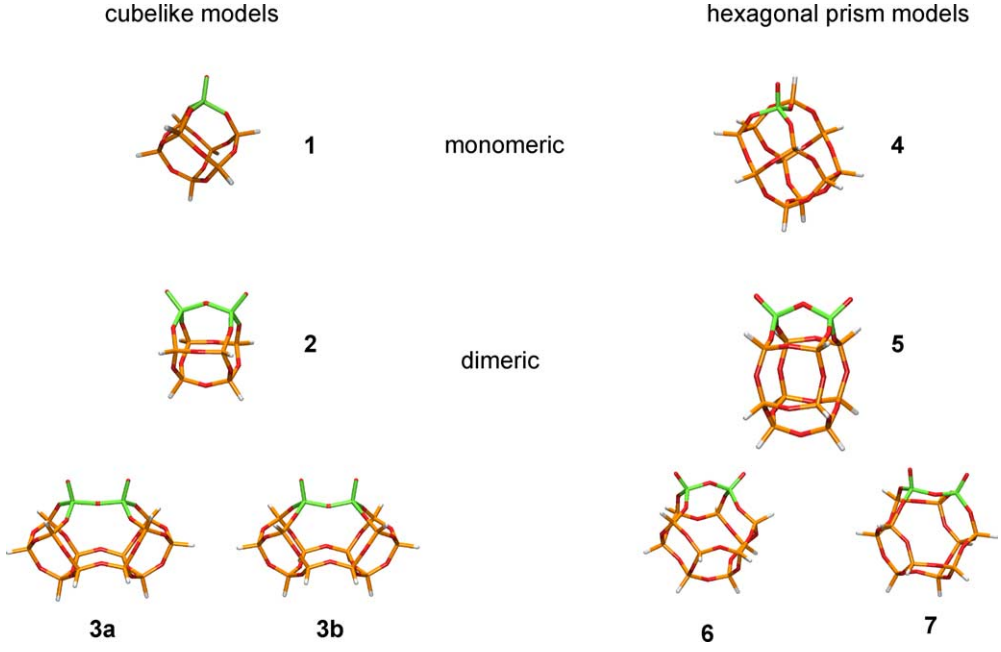

Fig. 2. Models for silica-supported vanadium oxide.

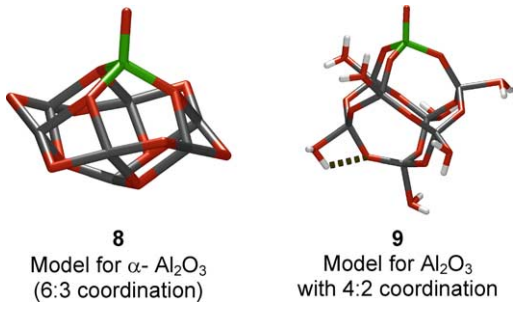

Fig. 3. Models for alumina-supported vanadium oxide.

substituents at the silicon atoms and was synthesized and characterized by Feher et al. [18]. In addition to the isolated site it is also possible to substitute two adjacent Si–H groups by V=O to give **2**. This is a simple model for a dimeric site with an O=V–O–V=O unit. However, the arrangement of the V=O groups is somewhat strained in this cubic model, so that the two V=O groups are not collinear. To avoid this we have designed model **3**. This model can be derived from two cube-like structures **1** by removing a Si–H corner of each cube and joining the dangling oxygen atoms. The result is a larger model, $V_2Si_{12}O_{23}H_{12}$, with a dimeric vanadia species and two nearly collinear V=O units. The model can either be considered with the structure constrained to the point group C_{2v} (**3b**) or without symmetry constraints (**3a**). Such cube-like structures are quite strained due to the fused four-membered rings. In order to study the impact of this structural constraint on the vibrational spectra, we also employ a silsesquioxane model with a hexagonal prism structure. This unit is known to exist in zeolites, e.g., in faujasite [19]. The structure used in this study was cut from the bulk structure of faujasite, again terminating dangling bonds with hydrogen atoms to yield a structure with D_{3d} symmetry. As a first step a model (**4**) with an isolated V=O site is constructed. This model is similar to **1**. Therefore, the impact of the different arrangement of the interface atoms is studied. When considering two adjacent V=O sites, three different possibilities arise in the framework of this model. The first is to place the vanadium atoms in different six-membered rings (**5**), yielding an arrangement that is roughly similar to **2**. The placement of the second vanadium atom in the same six-membered ring as the first leads to the structures **6** and **7**. The structure **6** is again similar to **2**, while **7** resembles the arrangement in **3**.

For the study of alumina-supported vanadium oxide, two different cluster models are employed (see Fig. 3). The first one is derived from a Al_8O_{12} model for the α-alumina surface, which has an Al atom in the top and bottom surfaces [20]. The layer composition from top to bottom is Al–O3–Al3–O6–Al3–O3–Al. In this model one "surface" aluminum atom is replaced by V=O to give a cluster with the composition $O{=}VAl_7O_{12}$ (**8**). In addition, a model is used in which aluminum is tetrahedrally coordinated and oxygen is twofold coordinated (**9**). This 4:2 coordination is found, for example, in the γ-alumina structure. This model has again a cube-like structure containing aluminum atoms at the vertices and oxygen atoms at the edges and to each aluminum atom, an additional water ligand is added. Thus, all aluminum atoms are in tetrahedral coordination and the framework oxygen atoms are connected to two aluminum atoms. By replacing one edge with V=O we arrive at model **9** with the composition $O{=}VAl_7O_{12}{\cdot}7H_2O$.

3. Experimental and computational details

3.1. Experimental model studies

The experiments on model catalyst systems presented in this work were performed in a multichamber UHV system operated at a base pressure below 2×10^{-10} mbar located at the Fritz-Haber-Institute. The system is equipped with all facilities necessary for sample preparation and characterization by scanning tunneling microscopy (STM), X-ray photoelectron spectroscopy (XPS), and infrared reflection-absorption spectroscopy (IRAS). This includes a variable temperature STM (Omicron), a dual-anode X-ray tube, and a concentric hemispherical analyzer (Scienta SES 200), as well as a Fourier-transform infrared spectrometer (Bruker IFS 66v/S) with a liquid nitrogen-cooled MCT detector. STM images were measured in the constant current mode, such that tunneling occurs between occupied tip and unoccupied sample states. Al-Kα-excited photoelectron spectra were recorded under normal electron emission with the analyzer set to a pass energy of 150 eV. For the acquisition of infrared spectra, p-polarized light was coupled into the UHV chamber via viton sealed KBr windows and reflected from the sample surface under grazing incidence. Spectral resolution after apodization was 3.3 cm^{-1}. Note that the metal surface selection rule [21] applies for the systems under discussion, owing to the limited thickness of the metal-backed oxide films.

Sample preparation was conducted in two steps, comprising the growth of the oxide films and the deposition of vanadium. The first step was performed according to the procedure published in the literature [22,23]. In the case of the alumina film, a sputter-cleaned NiAl(110) surface was exposed to $\sim$ 3000 L of O_2 (1 L = 10^{-6} Torr s) at 550 K and subsequently annealed at $\sim$ 1300 K [24]. In the case of the silica film, the Mo surface was cleaned via a combined oxidation and annealing procedure [16,25]. This is followed by four cycles of Si deposition from an electron-beam evaporator (EFM4, Focus) and subsequent oxidation at 900 K. Finally, the film is subjected to several annealing cycles, carried out in an oxygen ambient of 1×10^{-5} mbar and in the temperature range from $\sim$ 1100 to 1250 K [16,25]. After the preparation of the oxide films, their quality was checked by STM and LEED (low-energy electron diffraction). In a second step, vanadium (> 99.8%, Goodfellow) was deposited with the surface at 300 K and in an oxygen ambient of 1×10^{-7} mbar by means of an electron-beam

evaporator (EFM3T, Focus). During evaporation, the sample was held at a retarding potential to prevent vanadium ions from being accelerated toward the sample. A deposition rate of 0.36 ML per minute was determined with a quartz crystal microbalance. One monolayer of vanadium (1 ML V) was defined as the interlayer distance between the close-packed (110) planes of bulk vanadium of 2.14 Å, which corresponds to 1.54×10^{15} atoms cm^{-2}. Since the stoichiometry and morphology of the vanadia particles prepared might change with increasing vanadium loading, all coverages cited are expressed in terms of monolayers of vanadium metal deposited.

Adsorption of CO (> 99.997%, AGA) was carried out directly in the IR cell utilizing a gasdoser system while the sample was cooled to ∼ 90 K. In order to remove any contaminants from the gas feed, CO was passed through a cooling trap operated with liquid nitrogen. Note that CO does not adsorb on the clean oxide substrates at ∼ 90 K where all CO experiments on the vanadia particles have been conducted.

3.2. Powder samples

The vanadia on alumina sample was prepared by wet impregnation of ammonium metavanadate on δ-Al_2O_3 (100 m^2/g) to a loading of 1 wt% (ca. 1.2 V/nm^2). Pure mesoporous MCM-41 silica was prepared according to [26]. The BET surface area of pure MCM-41 was ca. 1010 m^2/g. The vanadia-supported MCM-41 (0.25 wt% of vanadium) was prepared in the following way. The vanadium precursor, i.e., vanadyl sulfate ($VO(SO)_4$) in water, was added along with tetraethylorthosilicate (TEOS) and cetyltrimethyl ammonium bromide (CTAB), with the latter being templates used for the preparation of MCM-41. The solution was stirred for 24 h at 300 K and subjected to further filtration and drying. The final catalyst was obtained by calcination at 823 K for 4 h. The BET surface area of V(0.25 wt%)-MCM-41 was ca. 1060 m^2/g resulting in the vanadium density of ca. 0.03 V/nm^2. Raman spectra were measured at Northwestern University using a controlled atmosphere fluidized-bed reactor that has been described previously [27]. The samples were calcined in the reactor with 5% O_2 in flowing N_2 at 823 K and then measured in flowing helium for V/Al_2O_3 and O_2/N_2 for V/MCM-41 at room temperature. Raman spectra of 1% V/alumina were measured using both visible laser excitation at 488 nm and ultraviolet laser excitation at 244 nm. Raman spectra of 0.25% V/MCM-41 were measured using 244 nm excitation.

3.3. Computational details

All calculations were performed in the frame of density-functional theory (DFT) using the software Turbomole 5.6 [28,29] by the group at Humboldt University Berlin. The calculations employed the gradient-corrected B-P86 [30,31] functional in conjunction with the triple-zeta valence plus polarization basis set of Ahlrichs et al. (TZVP) [32]. The resolution of identity (RI) method [33] was used to speed up the calculations. For all structures considered, structural optimizations were performed. Vibrational frequencies were calculated in the harmonic approximation with analytical second derivatives of the energy [34]. All calculated structures with the exception of **3b** correspond to minima on the potential energy surface. For the calculation of infrared intensities, $(d\mu/dq)^2$ was calculated by linear transformation of analytical Cartesian dipole derivates. All frequency calculations were performed for perdeuterated species in order to suppress spurious coupling of the V–O-stretching vibrations with Si–H bend modes. For the (4:2)-alumina model **9**, D_2O was used in the frequency calculation to decouple water bending vibrations from the V–O-stretching modes.

4. Results and discussion

The following four sections present and discuss the results from our structure analysis (STM, XPS, IRAS) and from our CO adsorption studies (IRAS) on model systems of vanadia on silica and alumina. For the case of VO_x/Al_2O_3, these aspects have already been thoroughly investigated before [22,35] so that we will focus here on silica-supported vanadia and, in particular, on the comparison between the two systems. The following sections contain the computational results and the Raman spectra of the powder samples, as well as a comparative discussion.

4.1. Experimental model studies

According to our STM measurements, small particles with very similar geometric structural properties are grown on alumina and silica under the preparation conditions applied. This is demonstrated in Fig. 4 for an intermediate V coverage. Obviously, spheroidal particles are generated with a homogeneous distribution over the support surface. As a result of the interaction with the oxygen ambient, large particle number densities, i.e., small particles, are formed [22].

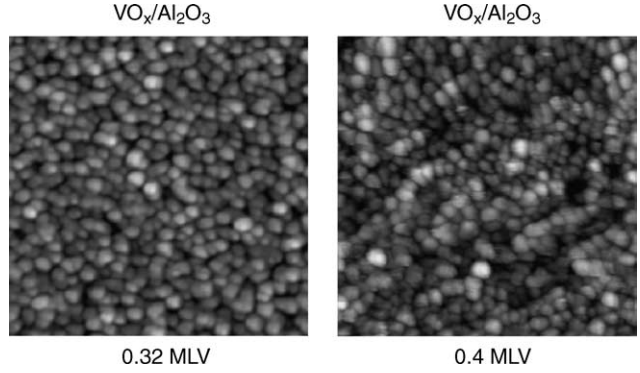

Fig. 4. Comparison of two STM images (50 × 50 nm) measured for alumina- and silica-supported vanadia particles of similar V content. Tunneling was performed at the following conditions: $U = 2.2$ V, $I = 0.07$ nA (VO_x/Al_2O_3); $U = 3.3$ V, $I = 0.12$ nA (VO_x/SiO_2). In both cases, particle number densities between ∼ 1.8 and 1.9×10^{13} particles per cm^{-2} were determined.

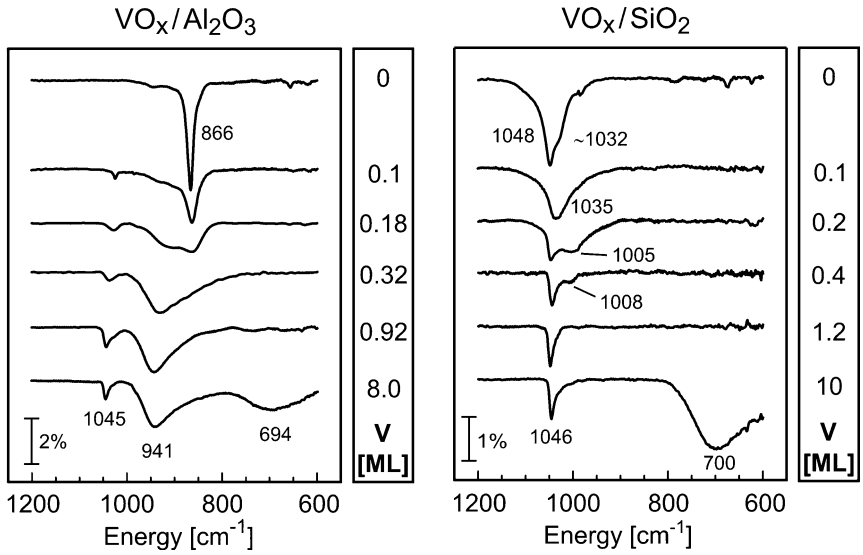

Fig. 5. IR spectra from alumina- and silica-supported vanadia particles as a function of V coverage. All spectra were measured at 300 K and referenced to the underlying NiAl and Mo metal substrates, respectively.

Typical particle diameters are in the range of 20–30 Å, but, owing to STM tip convolution effects, these values are generally overestimated by up to a factor of 2 [36]. As an alternative measure for particle sizes, the number of V atoms per particle is calculated from the amount of vanadium deposited and the determined particle number densities. It turns out that, at low V exposures, particles are produced which consist of only 1–2 V atoms on average. Upon increasing coverage, the particles continuously grow in size. At 1 ML V, for example, they contain ∼ 85 V-atoms. In order to get information on the vanadia oxidation state, XPS spectra have been recorded in the region of the O 1s and V 2p-binding energies. The V $2p_{3/2}$-binding energies are quite similar on both supports, being ∼ 0.15 eV higher on alumina than on silica. Presumably, this is due to large differences in the background intensity from NiAl and Mo substrate electrons. For high V coverages, the V $2p_{3/2}$ peak positions adopt values (VO_x/Al_2O_3, 515.5 eV; VO_x/SiO_2, 515.4 eV), which are close to the literature value of 515.7 eV for vanadium in the +3 oxidation state [37]. Note that for submonolayer coverages, shifts to higher binding energies are induced by final state and possibly also by initial state effects [22,23,35]. Perhaps a comment on the determined average oxidation state of +3 is appropriate at this point. We know from high-resolution photoelectron spectroscopy studies using synchrotron radiation that a single crystal V_2O_3 is characterized by V $2p_{3/2}$ bands whose shift is in agreement with V+3. However, as we showed before [38], the $V_2O_3(0001)$ surface of such a crystal is terminated by V=O groups rendering the oxidation state of the $V_2O_3(0001)$ surface as V+5. This is only detectable if on a flat surface photoelectron spectra at grazing take-off angles are taken, otherwise the average oxidation state detected is V+3. We suspect that a similar situation is also found here, but in the present case angle-resolved experiments with XPS are not expected to reveal the surface termination due to the particular morphology of the system (Fig. 4).

Finally, we have investigated the vibrational properties of our model systems, in order to derive information on the inner structure of the oxide particles. Fig. 5 presents a series of IR spectra measured as a function of vanadia loading. Although the results for VO_x/Al_2O_3 have been discussed in detail previously [22], they shall briefly be summarized again. The starting point is a clean alumina film, which is characterized by several sharp phonon bands, the most prominent of which is located at 866 cm^{-1}. Upon increasing V exposure, this feature attenuates very rapidly, indicating a strong interaction between vanadia and alumina. Concomitantly, two new signals appear at higher vibrational energies whose intensities saturate after ∼ 1 ML V. For multilayers, a third signal was detected at ∼ 700 cm^{-1}, which can be assigned to vibrations of a V–O–V bulk-species. A similar feature has been observed on thick V_2O_3 films grown on Pd(111) [39]. In contrast, the two other vibrations must be localized either at the surface of the vanadia particles or at their interface to the alumina support. Comparison with literature data revealed that the highest frequency band which shifts from ∼ 1025 to ∼ 1045 cm^{-1} with increasing V exposure, is due to terminating vanadyl groups (V=O) [4,40]. The band at ∼ 941 cm^{-1} involves vibrations of Al, O, and V ions (Al–O–V) [41]. This vibration is restricted to the interface region and is a result of strong vanadia–alumina interactions. CO experiments performed on this system provided further evidence for these assignments [23,35].

IR spectra for VO_x/SiO_2 are shown in Fig. 5 (right). The clean silica film is dominated by a narrow phonon band at 1048 cm^{-1} with a shoulder at lower energy. Upon vanadium deposition, these Si–O vibrations attenuate and broaden, while their frequency shifts to ∼ 1035 cm^{-1}, and finally to ∼ 1005–1008 cm^{-1} (note that these shifts are quite large as

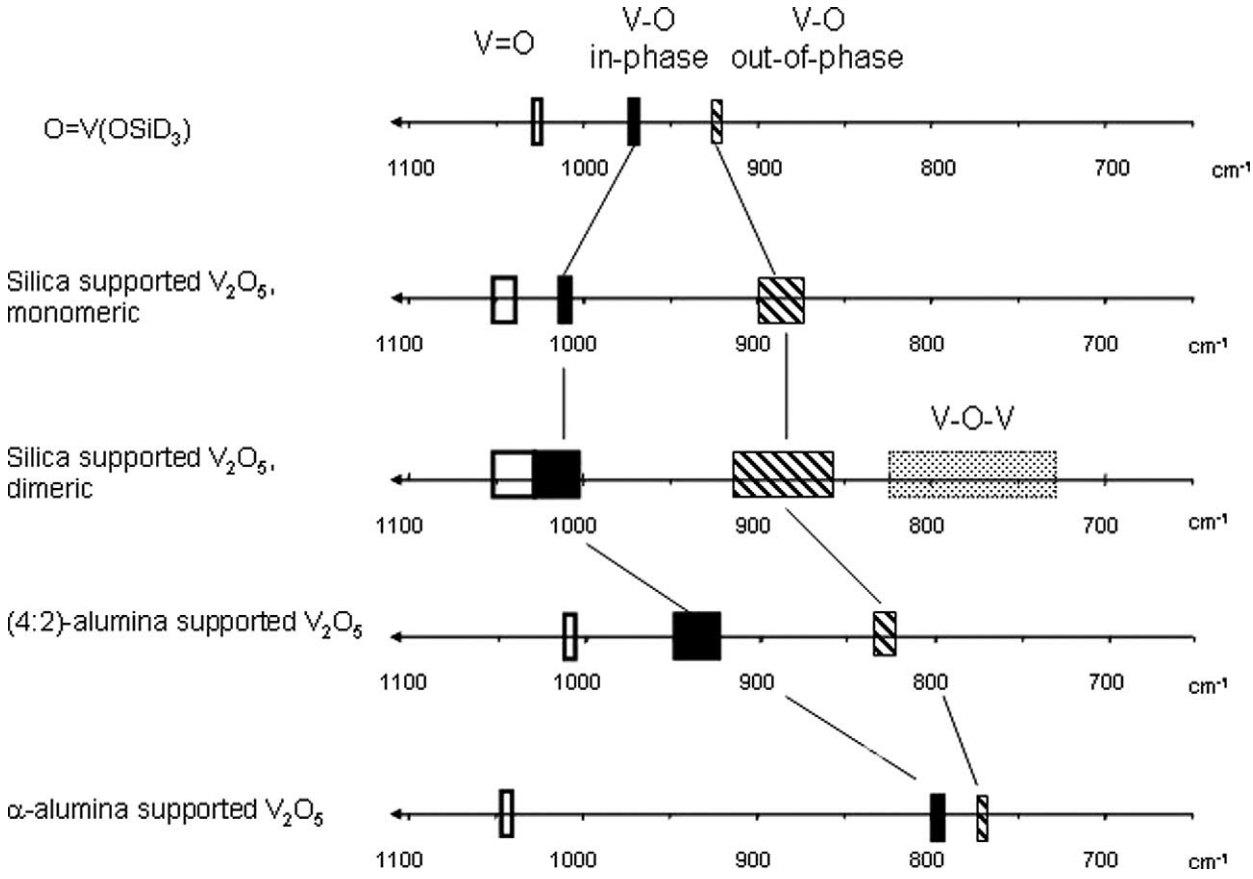

Fig. 6. Frequency ranges for V–O-stretching vibrations of models for different species and different supporting oxides.

compared to phonon shifts observed on alumina [42] but are similar to those found for UHV-deposited vanadium on silica [23,35]). After 0.4 ML V, the Si–O band has nearly disappeared. The same is true for the characteristic silica LEED pattern, which has become very faint with a high background intensity. Simultaneously, a new species has appeared at $\sim 1046\ \mathrm{cm}^{-1}$ whose properties—peak position and width, interaction with adsorbed CO [23,35]—correspond to those of the V=O groups on VO_x/Al_2O_3. At very high coverages, a V–O–V bulk species is observed in the same frequency regime as on alumina, thus underlining the similarity between the two systems.

Note, however, that the situation is more complicated in the case of VO_x/SiO_2 than it seems on first sight. This is due to the proximity of V=O and Si–O vibrations which might couple with each other. In addition, DFT calculations on model components **1**–**7** predict intense Si–O–V vibrations with frequencies in the range of ~ 1000–$1030\ \mathrm{cm}^{-1}$ (Fig. 6). These in-phase symmetric stretching vibrations should be visible in our IR spectra and one might suspect that the signal detected at $\sim 1005\ \mathrm{cm}^{-1}$ represents species of that kind instead of attenuated Si–O vibrations. However, its intensity development is completely different from that of the Al–O–V mode, as evidenced by Figs. 5 and 7. While the band on silica vanishes at intermediate V coverages, the Al–O–V band grows until an exposure of ~ 1 ML V and remains constant thereafter [22].

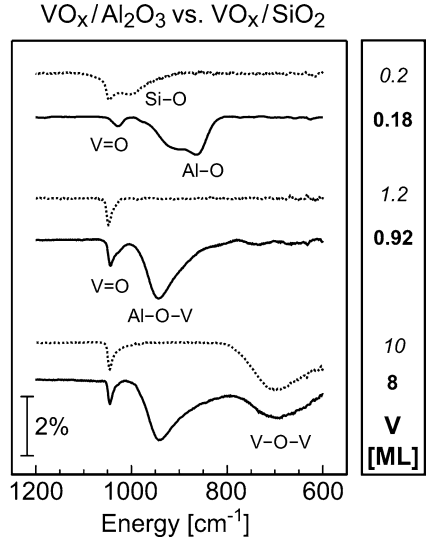

Fig. 7. Comparison of spectra taken from Fig. 5 for specific V coverages. Solid line, VO_x/Al_2O_3; dotted line, VO_x/SiO_2.

In conclusion, we can neither prove nor exclude the presence of Si–O–V interface modes in our IR spectra on the basis of the experiments so far. Nevertheless, it is clear that the interaction between vanadium and the oxide support is con-

siderably weaker for VO_x/SiO_2 than for VO_x/Al_2O_3. This is corroborated by experiments where isolated vanadium carbonyls were generated on both oxide films. On alumina, this was possible at a temperature of 300 K, while for silica the sample had to be cooled to 90 K in order to reduce the diffusion length of deposited V atoms to such an extent that a sufficient number of single atoms was formed [23,35,43]. The results on CO adsorption described below as well as the results of the calculations reported in the next section corroborate the conclusions so far.

Fig. 8 presents IR spectra for CO-saturated vanadia on alumina and silica. Remarkable differences are obvious. For VO_x/SiO_2, only one CO species is visible at a constant frequency and with a monotonous intensity evolution. In contrast, four different species can be distinguished for VO_x/Al_2O_3. Only one of them exists in the whole V-coverage regime while the others are restricted to submonolayer loadings. Interestingly, two species possess frequencies which are red-shifted with respect to the CO gas-phase value (2143 cm^{-1}) [44], indicating an influence of defect sites. For the species at 2031 cm^{-1}, this could be shown in a separate set of experiments [23,35]. As outlined in Fig. 9, there are other differences between alumina- and silica-supported vanadia, such as the strong frequency shifts of two of the CO species and, most notably, the pronounced maximum in the integral CO absorption intensity at an intermediate coverage of ∼ 0.3 ML V (note that this maximum in the IR intensity is indeed correlated with a maximum amount of CO adsorbed [23,35]).

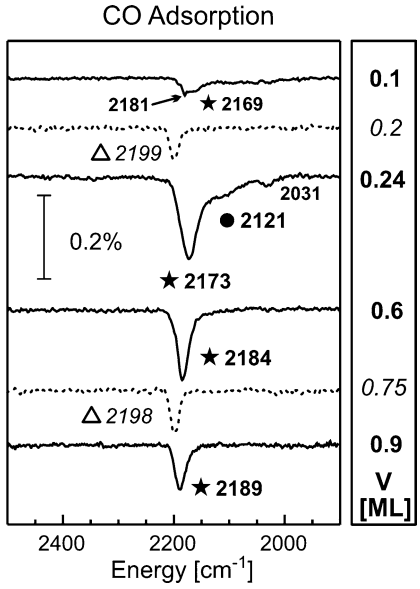

Fig. 8. IR spectra taken from CO saturated vanadia particles of different V contents. CO exposure was performed at 90 K. Solid line, VO_x/Al_2O_3; dotted line, VO_x/SiO_2. The symbols provided next to some of the frequency values correspond to those used in Fig. 9.

According to our previous investigations [23,35], strong interactions at the vanadia–alumina interface are most likely responsible for this complex adsorption behavior on VO_x/Al_2O_3. This conclusion is based on the observation that all the peculiarities under discussion occur at submonolayer V coverages where adsorbed CO has access to the interface region. In fact, characteristic frequency shifts of the Al–O–V interface vibrations are observed at low vanadia loadings and can be regarded as a direct evidence for a mutual influence between CO molecules and specific interface structures. Possibly, these structures are formed via substitution of Al ions at the alumina surface by V ions. Such defects are likely to be present since we know from our STM analysis [22] that the vanadia aggregates are partially incorporated into the alumina film. Moreover, such defects are expected to lead to the observed, red-shifted CO frequencies [45]. To identify the specific nature of these interface structures, DFT calculations were performed for thin vanadia films on α-Al_2O_3 [46]. The 866 cm^{-1} of the alumina support and the 941 cm^{-1} of the interface mode indicate the presence of 4-fold coordinated Al; the alumina film employed has, indeed, a structure similar to γ-Al_2O_3 [11] with Al in tetrahedral sites. DFT calculations performed on model **9** with Al

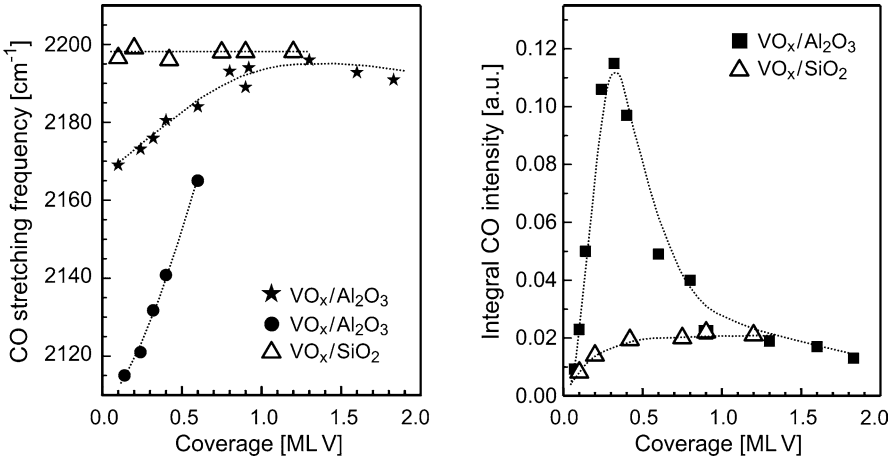

Fig. 9. Analysis of the frequency and intensity development of CO species observed in the IR spectra after saturation of alumina- and silica-supported vanadia particles.

ions in tetrahedral coordination predict intense in phase V–O (interface)-stretching modes in the range 926 to 955 cm^{-1}.

Regarding the proposal of an interface-driven adsorption behavior for VO_x/Al_2O_3, the comparison to VO_x/SiO_2 is of particular importance as it provides a means to study the same particles but with reduced support interactions. One would expect in this case only weak dependencies on the vanadia loading. This is exactly what we have observed for silica-supported vanadia; i.e., there are no extra CO peaks at low V coverages, and the absorption intensity shows only a simple saturation behavior. Furthermore, the CO spectra are very similar on both systems at coverages above ~ 1 ML V where the interface is unaccessible and CO adsorption is dominated by the properties of the vanadia overlayer itself.

To summarize, we have prepared vanadia particles both on alumina and on silica thin-film supports. According to STM, XPS, and IRAS, these particles exhibit very similar structural properties with respect to the average particle size (20–30 Å), the average oxidation state (3+) and the presence of V=O and V–O–V structural elements. However, there is one major difference between the two systems: the extent of particle–support interactions. These are very strong for VO_x/Al_2O_3, as evidenced, for example, by the formation of an intense Al–O–V interface species. Much weaker interactions are observed for VO_x/SiO_2 and hence only weak Si–O–V vibrations. Most interestingly, these structures in the interface region are found to strongly affect the CO adsorption properties of the whole system, regarding the number of CO species existing, as well as their frequency and intensity behavior as a function of the vanadia loading.

4.2. Cluster models

Tables 1 and 2 show the frequencies and intensities obtained for models of vanadium oxide supported on silica and alumina, respectively. Fig. 6 compares the frequency ranges for different species.

For the $O{=}V(OSiD_3)_3$ molecule three different bands can be distinguished. At the high-frequency end as expected the vanadyl stretch is found at 1035 cm^{-1}. The vibrations of the three V–O–Si oxygen atoms are coupled and give rise to an in-phase motion (979 cm^{-1}) and a degenerate pair of out-of-phase modes at 932 cm^{-1}. The latter is by far the most intense. These results are in very good agreement with the observed IR and Raman spectra of the $O{=}V(OSi(O^tBu)_3)_3$ molecule [17]. The Raman spectrum shows the vanadyl stretch at 1038 cm^{-1} (in the IR hidden by very intense Si–O–C stretches) and the IR spectrum shows the V–O–Si out-of-phase modes as an intense pair at 920/910 cm^{-1}.

Table 2
Vibrational frequencies of models for alumina-supported vanadium oxide

Model	**8**		**9**	
	Frequency	Intensity	Frequency	Intensity
V=O stretch	1047	244	1012	17
In-phase V–O (interface) stretch	796	236	955	1073
			951	1188
			937	654
			926	338
Out-of-phase V–O (interface) stretch	771	0	838	124
	771	0	825	101

Note. Frequencies in cm^{-1}, intensities in km/mol.

Table 1
Calculated vibrational frequencies of models for silica supported vanadium oxide

	$O{=}V(OSiD_3)_3$	**1**	**4**	**2**	**3a**	**3b**	**5**	**6**	**7**
V=O stretch									
Frequency	1035	1047	1043	1050	1045	1046	1047	1046	1048
Intensity	100	473	369	318	257	110	158	237	520
Frequency				1041	1033	1033	1037	1037	1037
Intensity				368	132	90	315	259	196
In-phase V–O (interface) stretch									
Frequency	978	1011	1008	1014	1009	1031	1015	999	1010
Intensity	20	291	349	973	891	1093	977	1169	1052
Out-of-phase V–O (interface) stretch									
Frequency	932	877	897	895	890	906	924	887	893
Intensity	1033	191	384	354	331	322	693	394	397
Frequency	932	877	868	865	883	898	878	869	875
Intensity	1033	191	181	0	16	0	7	119	170
V–O–V stretch + out-of-phase V–O (interface) stretch									
Frequency				981	989	1000	975	969	986
Intensity				126	23	47	123	40	70
V–O–V stretch									
Frequency				766	822	819	737	777	795
Intensity				442	1373	1371	417	639	666

Note. Frequencies in cm^{-1}, intensities in km/mol.

The splitting is obviously due to a small deviation of this molecule from the threefold symmetry. The in-phase V–O–Si mode is not seen in the IR spectrum because of its very low intensity and also not observed in Raman.

For monomeric vanadium oxide species on silica (models **1** and **4**), the same three bands are found. The vanadyl stretch is between 1050 and 1040 cm^{-1}. The vibrations of the three V–O–Si interface oxygen atoms are again coupled into an in-phase motion and two out-of-phase modes. The frequency for the in-phase mode is around 1010 cm^{-1} with only a slight difference between the two different models. The frequencies of out-of-phase interface modes show a stronger dependence on the model choice. One is shifted by more than 20 cm^{-1} between **1** and **4**. This change can be attributed to the different V–O–Si angles in the two compounds. When looking at the intensities of the vibrational modes it is evident that the changes are larger than for the frequencies. Thus, the intensities are more dependent on details of the structures. It seems also safe to assume that the accuracy of the DFT calculations is lower for IR intensities than for vibrational frequencies.

Comparison of the $O{=}V(OSiD_3)_3$ molecule with the polyhedral silsesquioxane models **1** and **4** reveals significant changes which are much larger than the changes between models **1** and **4**. The splitting between the in-phase and out-of-phase V–O–X interface modes becomes much larger in models **1** and **4** than in the $O{=}V(OSiD_3)_3$ molecule (Fig. 6) and their intensity becomes much more similar. The in-phase mode is blue shifted for models **1** and **4** (above 1000 cm^{-1}) and is very close to the region of the vanadyl vibration.

For the dimeric vanadium oxide species (models **2**–**3** and **5**–**7**), the situation is more complex. The two vanadyl-stretching vibrations are coupled into in-phase (around 1045 cm^{-1}) and out-of-phase modes (around 1035 cm^{-1}) with splittings between 9 and 13 cm^{-1}. The intensities differ considerably for the different models and no systematic trend can be seen. However, for all models of the dimeric species the sum of the intensities is lower than twice the intensity of the vanadyl band for the corresponding models of monomeric species. This indicates that the intensity of the vanadyl band may vary substantially between different species while all frequencies are in a range of 17 cm^{-1}. Hence, the use of the vanadyl band for normalization of experimental spectra might be dangerous.

The in-phase V–O–Si mode is found between 1000 and 1030 cm^{-1}. For most models it is around 1010 cm^{-1}, the highest wavenumber (1030 cm^{-1}) is found for model **3b** (C_{2v} symmetry, no minimum structure) and the smallest for model **6** (999 cm^{-1}). Compared to the monomeric species for this mode the changes of the vibrational frequency are quite small, but the impact on the intensity is huge. For the dimeric species (all models), the intensities are consistently larger by a factor of two to three. As a result, the intensities predicted for dimeric species become larger for the in-phase V–O–Si interface mode than for the vanadyl modes. In addition, DFT tends to overestimate the frequency of the V=O-stretching mode and it seems possible that in experiment the vanadyl band and the intense in-phase band might overlap. The behavior of the out-of-phase coupled V–O–Si interface modes is similar to the monomeric species. Only two instead of the expected three modes are found, the third mode is coupled with the motion of the V–O–V-bridging oxygen atom and is found at higher frequency (see below). The frequencies and intensities are comparable with those of the monomeric species.

For the dimeric species the vibration of the bridging oxygen atom, V–O–V, must also be considered. Inspection of the vibrational modes revealed that the V–O–V oxygen atom is involved in two modes. One is the V–O–V vibration and the other one has V–O–V and V–O–Si contributions. The latter mode is found between 1000 and 970 cm^{-1} and is of moderate intensity only. The frequency of the unperturbed V–O–V mode is quite dependent on the arrangement of the V–O–V unit and falls into the range 735 to 825 cm^{-1}. The different models for dimeric species can be divided into two classes. In one class, the bridging oxygen atom points away from the cage structure which is the case for models **2**, **5**, and **6**. For these structures, the V–O–V modes are at the low end of the frequency range. To the other class belong models **3a**, **3b**, and **7** in which the bridging oxygen atom points toward the cage. For the latter class the V–O–V mode is at the high end of the 735–825 cm^{-1} range. The intensities of the V–O–V mode are quite high. Indeed, for models **3a** and **3b** this mode is the most intense of the vibrations involving the vanadium oxide part. Despite its high intensity this mode is probably very hard to detect in IR experiments as this region of the spectrum is usually dominated by framework vibrations of the silica support.

The results indicate that it will be difficult to distinguish between monomeric and polymeric species by infrared spectroscopy, as the overall vibrational behavior is similar (Fig. 6). The differences in the frequencies are relatively small. One difference is the higher intensity of the in-phase V–O–Si mode for dimeric species, but this band might be difficult to detect due to overlap with the vanadyl band. The other one is the V–O–V mode, which is covered by vibrations of the silica support.

For alumina-supported vanadium oxide at first a cluster model for α-alumina (**8**) was considered. Again, three different bands are expected. The vanadyl frequency is at 1047 cm^{-1} with a slightly lower intensity than on silica support. For the vibrational modes of the interface oxygen atoms, the in-phase coupling (796 cm^{-1}) and the out-of-phase coupling (two degenerate bands at 771 cm^{-1}) can be distinguished. For the interface modes, some coupling to the interface modes of the aluminum "surface" atom at the backside of the cluster is visible. This is an indication that properties (e.g., bond length, force constants) of the "surface" aluminum atom and the vanadium atom are similar. The results are in agreement with a calculation applying periodic boundary conditions for V_2O_5 films on α-alumina [46]. Even for the (0001) surface of α-alumina the Al_8O_{12}

model reproduces the Al–O mode at the surface quite well, 909 cm^{-1} compared to 915–888 cm^{-1} for the periodic slab model (PW91 functional).

The change to model **9**, which contains tetrahedrally coordinated aluminum and twofold coordinated oxygen atoms, has a dramatic influence on the vibrational spectrum. The vanadyl band is red shifted by more than 30 cm^{-1} compared to **8**. This change can be understood in terms of the interaction of the vanadium atom with the interface oxygen atoms. In **8,** this interaction is weaker because the oxygen atoms are in threefold coordination. This is also indicated by different V–O distances, which are 179.3 pm for **8** and 177.1 to 178.3 pm in **9**. Due to the stronger interaction with the V–O–Al oxygen atoms in **9** the vanadyl bond gets weaker and, hence, longer: 159.9 pm (**8**) and 161.4 pm (**9**). A similar effect is also seen on the vibrational frequencies of the V–O–Al interface mode, which are blue-shifted with respect to **8**, indicating a stronger interaction. However, the interpretation is more complicated for **9** as there is a strong vibrational coupling between the in-phase V–O–Al interface mode and the remaining Al–O–Al framework vibrations. As different couplings are possible, more than one mode, which involves the V–O–Al interface, occurs. The four most intense modes, which are given in Table 2, fall in the region between 955 and 925 cm^{-1}. These bands have a high intensity so that a band can be expected in this region of the infrared spectrum. A strong band is indeed seen at 941 cm^{-1} in the IRAS spectra for vanadium oxide supported on alumina films which are known to have aluminum in tetrahedral sites (Fig. 5, [22, 35]). When comparing **8** and **9** it is evident that the anchoring of the vanadium atom by twofold instead of threefold coordinated oxygen atoms results in a blue shift of 150 cm^{-1} of the interface mode.

Finally, the out-of-phase motion for the interface oxygen atoms leads to bands at 838 and 825 cm^{-1}, so that the blue shift with respect to **8** is a lot smaller in this case. As the out-of-phase V–O–Al vibrations do not couple with Al–O–Al modes one should assume that the large change in the in-phase mode between **8** and **9** is partly a result of the cooperative motion of the V–O–Al and Al–O–Al oxygen atoms.

4.3. Powder samples

The Raman spectra obtained from vanadia/δ-alumina and V/MCM-41 samples are shown in Fig. 10. The spectra from vanadia/δ-alumina clearly depend on the excitation wavelength. With 488 nm excitation the vanadia/δ-alumina sample exhibits a single peak in the Raman spectrum at 1031 cm^{-1} that has been assigned in the literature to isolated, monomeric, vanadyl groups [1–4,10]. Under 244 nm excitation the Raman spectrum from vanadia/δ-alumina exhibits a relatively narrow band at 1022 cm^{-1} and a broad band centered at 915 cm^{-1}. For V/MCM-41 a pair of narrow peaks at 1035 and 1065 cm^{-1} are observed. The differences in 488 and 244 nm excited Raman spectra of vanadia/δ-alumina are not due to laser-induced changes in the sample.

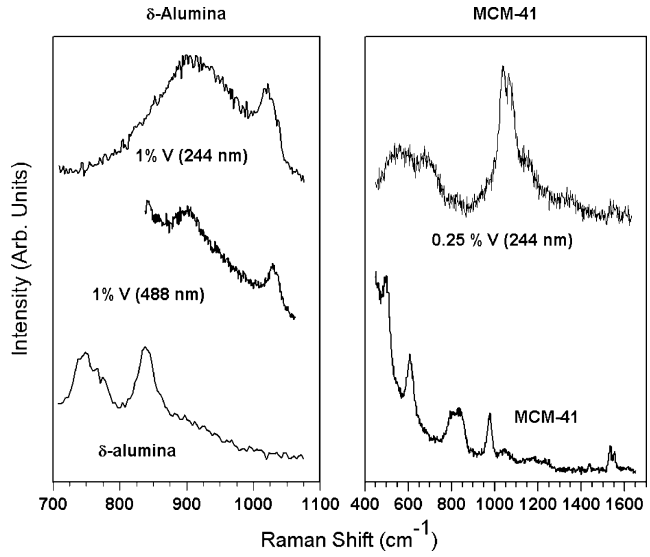

Fig. 10. Comparison of 488 and 244 nm laser excited Raman spectra from 1% vanadia/δ-alumina, 0.25% V/MCM-41, and the pure supports.

Spectra were recorded under a controlled atmosphere and using a variety of conditions, including an experiment where the two lasers simultaneously irradiated the same area of the sample. There was never any indication of laser-induced changes to the sample.

In the literature broad bands in the 750–1000 cm^{-1} region are assigned to V–O–V stretches in two-dimensional polyvanadates. Sharp Raman bands in the range 900–1050 cm^{-1} have been assigned to the V=O-stretching vibration. The frequency of V=O has been reported to follow both the order polymerized V > isolated V > V_2O_5 [4,47–50] and the order isolated V > polymerized V > V_2O_5 [50]. The measured Raman spectra excited at 488 and 244 nm show that different surface V species and possibly different oscillators are detected at the two excitation wavelengths. Previously, a band at 1031 cm^{-1}, observed here under 488 nm excitation from the vanadia/δ-alumina sample, has been attributed to isolated vanadyl species that were presumed to be the only species present on a low-loading sample [3]. The infrared spectra on the model catalysts prove that a band at this frequency is also produced by cluster vanadyl species. Moreover, the 244 nm Raman spectrum demonstrates the presence of vanadia species that are not detected under 488 nm excitation. The band detected at 1022 cm^{-1} under UV excitation has also been attributed to isolated V=O species; however, our measured difference in Raman shift indicates that this surface vanadyl is distinct from the species detected by visible laser excitation. It was observed even on vanadia/alumina with a loading of only 0.06%. The fact that Raman spectra change with excitation wavelength is further confirmed by the results from V/MCM-41. Since MCM-41 is a mesoporous silica, the analogous material studied previously is vanadium oxide supported on amorphous silica. Several groups have reported Raman spectra from V/SiO_2 with a single band at 1035–1050 cm^{-1} at low vanadium

loading, attributed to isolated V=O [10,40,51–53]. However, when using 244 nm excitation a band at 1065 cm^{-1} is observed in addition to the band at 1035 cm^{-1}.

The phonon spectra of δ-alumina and MCM-41 supports measured by 244 nm Raman spectroscopy are also compared in Fig. 10. The higher phonon frequencies in the silica support are evident. Differences in the calculated coupling between surface V=O oscillator and the phonons in the two supports lead to peak shifts and splittings observed in the Raman spectra.

4.4. Comparison between experimental and theoretical model studies

Figs. 6 and 7 are best suited for a comparative assignment of the vibrational spectra. In Fig. 6 we mainly use the calculated frequency ranges for the models represented in the second/third and in the fourth line from above. It is clear that in both cases, i.e., vanadia on silica and vanadia on alumina, the sharp band above 1000 cm^{-1} is connected with the vibration of the vanadium oxygen double bonds in the vanadyl groups. However, in the case of silica, in particular, there is a strong coupling with the vanadia–silica interface modes, which appear in the same range of frequencies because the frequency of silica modes is situated in this energy range. This is revealed by the experimental spectra in the model studies and by the calculations. In fact, it is not possible to assign the spectral features in this energy range for silica substrates solely to the vibration of vanadyl groups and therefore shifts in the frequency of this band cannot simply be interpreted as being due to a change in the bond strength or bond length of the vanadium oxygen double bond as is often done in studies of powder catalysts. On the other hand, for the vanadia–alumina system the interface modes are separated in energy from the vanadyl vibrations, occurring in the range 940–950 cm^{-1}, as deduced from the model experiments and here for the first time corroborated by theoretical calculations. Again, the reason can be found in the fact that the substrate alumina vibrations are situated in the spectral range near 900 cm^{-1}, as opposed to a range above 1000 cm^{-1} for silica. When comparing experimental and theoretical results we have to keep in mind that the experimental studies were carried out on systems where vanadia silica/alumina films were prepared on top of a metal substrate. In such a case, the so-called surface selection rules apply in infrared spectroscopy. This implies that all modes with a dynamic dipole parallel to the surface are screened and will have very low or no intensity in the infrared spectrum. It is therefore very reasonable to assume that the calculated out-of-phase vibrations do not show up in the experimental spectrum unless there is a systematic change in geometry. Based on Figs. 6 and 7 we can now come to a consistent assignment of both vanadia–silica and vanadia–alumina spectra. It is obvious that the band in the 950 cm^{-1} range is due to interface modes and does not originate from internal vibrations of the V–O–V type, as they would be typical for polymeric vanadia species. The latter species lead to bands located at 700 cm^{-1} as shown in Figs. 6 and 7. In fact, it turns out that it will be very difficult to use vibrational spectra with the typically achieved resolution on catalyst samples to differentiate monomeric and polymeric species. The interface modes that can be clearly differentiated from the vanadyl vibrations for the vanadia–alumina case are shifted upward in energy for the case of vanadia–silica systems so that in the latter case a clear differentiation even between vanadyl vibrations and interface modes cannot be made.

We have applied the above-developed assignment of the vibrational spectra to study real powder samples. Typically in those cases Raman spectra are available. Infrared spectra are very scarce because the spectra are swamped by the substrate modes. Most Raman spectra in the literature have been taken using visible light, and only recently, UV-Raman spectra are becoming available. The spectra of V/alumina (δ) and V/silica (MCM-41) are reported in Fig. 10. Also, most sets of data have been recorded for vanadia–alumina systems and there is very little systematic study for different supports. The assignments reported in the literature are based upon a differentiation of monomeric and polymeric species (Fig. 1) by evaluating the presence or absence of the band in the range of 950 cm^{-1} and shifts of the vanadyl band, which is always treated as being isolated and independent of the other vibrations in the system as we have discussed above. Such an interpretation is very dangerous and may lead to erroneous conclusions. In fact, interface modes between vanadia and the support have to be considered in addition to isolated and polymeric species to assign the spectra and the former allow interesting conclusions to be drawn on vanadia–support interactions. In order to substantiate these statements we refer to the measurement of powder spectra reported above. Both visible and UV-Raman spectra have been recorded in order not be mislead in the assignments. As we shall demonstrate in the following, those data fully support the above analysis and we believe that on the basis of the present study a new systematic study of vanadia-supported catalysts is in order and necessary.

Comparison of Figs. 7 and 10 documents the similarities in the main features between the IR spectra of the model systems (Fig. 7) and the Raman spectra of the powder samples (Fig. 10). For the silica-based system the absence of the feature at 950 cm^{-1} is clearly apparent, while the feature in this range of frequencies is prominent for the alumina-based vanadia samples. This is consistent with the interpretation that these features are mainly due to interface vibrations. If we assumed they were due to V–O–V vibrations as suggested in the literature [1–4,10], there would be no reason why they should be absent for the silica-based systems given the similarity of the morphology of the vanadia clusters for V/alumina and V/silica as demonstrated in Fig. 4. At this point, we therefore are forced to conclude that one cannot use this feature to assign properties of so-called “polymeric vanadia species.” It is also obvious that the sharp band above 1000 cm^{-1} cannot be assigned to vanadyl species exclu-

sively, as has also often been done in the literature [1–4,10]. In both sets of spectra, i.e., the model catalysts, as well as the powder samples, the coupling with the silica substrate is clearly observed. For example, it shows up in the powder Raman spectra as a split line, as predicted by the cluster calculations. However, the calculations also predict, in agreement with experiment, that for V/alumina the vanadyl vibration can be considered as an independent oscillator. Here it makes sense to address shifts of the vanadyl vibration as a function of the chemical environment, i.e., its involvement in monomeric and polymeric groups and its bonding to surface oxygens with twofold vs threefold coordinations. UV–vis absorption spectra measured from the V/δ-alumina sample show significant absorption bands at both 244 and 488 nm laser wavelengths, which implies that the Raman spectra are resonance enhanced. The longer wavelength absorption intensity increases with vanadia loading, relative to the short wavelength absorption. This demonstrates that a mixture of surface vanadia species is present and is consistent with a picture where polymeric vanadyl species are resonance enhanced under visible laser excitation and isolated vanadyls are resonance enhanced under ultraviolet laser excitation. Interestingly, the higher V=O Raman shift measured under visible compared to UV excitation is consistent with this picture by reference to the measurements on the model catalysts since the V=O infrared frequencies are found to increase with increasing V=O surface density [22]. Thus, it would appear that visible excited Raman spectra are more sensitive to polymeric or cluster vanadyls and ultraviolet excited Raman spectra are more sensitive to isolated vanadyl species.

5. Summary and conclusions

In the present study, we have combined experimental studies on model catalysts and on powder catalysts with cluster calculations to address the assignment of vibrational spectra of supported vanadia catalysts.

It turns out that it is possible to find a unique interpretation of spectra of model systems and powder samples based on the analysis of theoretical calculations. However, the findings are not completely consistent with the view generally discussed in the literature and we propose that this view must be revised.

In particular, the so-called vanadyl vibrations cannot, in general, be assumed to be independent of the substrate and thus cannot be used as an indicator for monomeric and polymeric species. In fact, it is much more the coupling of the vanadia to the support that has to be considered in the interpretation of the spectra. By using two different supports, namely silica and alumina, we prove the dominance of interface vibrations in both infrared and Raman spectra based on the results of cluster calculations in conjunction with morphological studies using the STM.

It is this combination of experimental techniques and calculations that allows us to draw conclusions on the correlation of structure and spectroscopy which otherwise are difficult or even impossible to reach.

Acknowledgments

The authors gratefully acknowledge financial support by the Deutsche Forschungsgemeinschaft (DFG) through the Sonderforschungsbereich 546. We also thank the Athena project funded by the EPSRC of the UK and Johnson Matthey plc. and the COMBICAT/Malaysia consortium for financial support. N.M. is grateful to the Studienstiftung des deutschen Volkes for a fellowship. J.B.G. thanks the Natural Sciences and Engineering Research Council of Canada. P.C.S. is grateful to the Alexander von Humboldt Foundation.

References

[1] G.C. Bond, S.F. Tahir, Appl. Catal. 71 (1991) 1.
[2] G. Deo, I.E. Wachs, J. Haber, Crit. Rev. Surf. Chem. 4 (1994) 141.
[3] B.M. Weckhuysen, D.E. Keller, Catal. Today 78 (2003) 25.
[4] I.E. Wachs, Catal. Today 27 (1996) 437.
[5] F.D. Hardcastle, I.E. Wachs, J. Phys. Chem. 95 (1991) 5031.
[6] A.M. Turek, I.E. Wachs, E. DeCanio, J. Phys. Chem. 96 (1992) 5000.
[7] G. Deo, I.E. Wachs, J. Phys. Chem. 95 (1991) 5889.
[8] B.M. Weckhuysen, I.E. Wachs, J. Phys. Chem. 100 (1996) 14 437.
[9] L.E. Briand, J. Jehng, L. Cornaglia, A.M. Hirt, I.E. Wachs, Catal. Today 2833 (2002) 1–12.
[10] A. Khodakov, B. Olthof, A.T. Bell, E. Iglesia, J. Catal. 118 (1999) 205.
[11] M. Bäumer, H.-J. Freund, Progr. Surf. Sci. 61 (1999) 127.
[12] H.-J. Freund, M. Bäumer, H. Kuhlenbeck, Adv. Catal. 45 (2000) 333–384.
[13] H.-J. Freund, Surf. Sci. 500 (2002) 271–299.
[14] H.-J. Freund, M. Bäumer, J. Libuda, T. Risse, G. Rupprechter, S. Shaikhutdinov, J. Catal. 216 (2003) 223.
[15] H.-J. Freund, J. Libuda, M. Bäumer, T. Risse, A.F. Carlsson, Chem. Rev. 3 (2003) 181–200.
[16] T. Schroeder, J. Giorgi, M. Bäumer, H.-J. Freund, Phys. Rev. B 66 (2002) 165 422.
[17] R. Rulkens, J.L. Male, K.W. Terry, B. Olthof, A. Khodakov, A.T. Bell, E. Iglesia, T.D. Tilley, Chem. Mater. 11 (1999) 2966.
[18] F.J. Feher, J.F. Walzer, Inorg. Chem. 30 (1991) 1689.
[19] C. Baerlocher, W.M. Meier, D.H. Olsen, Atlas of Zeolite Framework Types, Elsevier, Amsterdam, 2001.
[20] J.M. Wittbrodt, W.L. Hase, H.B. Schlegel, J. Phys. Chem. B 102 (1998) 6539.
[21] F.M. Hoffmann, Surf. Sci. Rep. 3 (1983) 107.
[22] N. Magg, J.B. Giorgi, T. Schroeder, M. Bäumer, H.-J. Freund, J. Phys. Chem. B 106 (2002) 8756.
[23] N. Magg, J.B. Giorgi, A. Hammoudeh, T. Schroeder, M. Bäumer, H.-J. Freund, J. Phys. Chem. B 107 (2003) 9003.
[24] R.M. Jaeger, H. Kuhlenbeck, H.-J. Freund, M. Wuttig, W. Hoffmann, R. Franchy, H. Ibach, Surf. Sci. 259 (1991) 235.
[25] T. Schroeder, A. Hammoudeh, M. Pykavy, N. Magg, M. Adelt, M. Bäumer, H.-J. Freund, Solid State Electron. 45 (2001) 1471.
[26] A.G. Grubert, J. Rathousky, G. Schulz-Ekloff, M. Wark, A. Zukal, Micropor. Mesopor. Mater. 22 (1998) 225.
[27] Y.T. Chua, P.C. Stair, J. Catal. 196 (2000) 66.
[28] R. Ahlrichs, M. Bär, M. Häser, H. Horn, C. Kölmel, Chem. Phys. Lett. 162 (1989) 165.

[29] O. Treutler, R. Ahlrichs, J. Chem. Phys. 102 (1995) 346.
[30] A.D. Becke, Phys. Rev. A 38 (1988) 3098.
[31] J.P. Perdew, Phys. Rev. B 33 (1986) 8822.
[32] A. Schäfer, C. Huber, R. Ahlrichs, J. Chem. Phys. 100 (1994) 5829.
[33] K. Eichkorn, O. Treutler, H.R.H. Öhm, R. Ahlrichs, Chem. Phys. Lett. 240 (1995) 283.
[34] P. Deglmann, F. Furche, R. Ahlrichs, Chem. Phys. Lett. 162 (2002) 165.
[35] N. Magg, Thesis, Humboldt Universität, 2003 (English language).
[36] S. Stempel, M. Bäumer, H.-J. Freund, Surf. Sci. 402–404 (1998) 424–427.
[37] G.A. Sawatzky, D. Post, Phys. Rev. B 20 (1979) 1546.
[38] A.-C. Dupuis, M. Abu Al-Haija, B. Richter, H. Kuhlenbeck, H.-J. Freund, Surf. Sci. 539 (2003) 99–112.
[39] M. Sock, S. Surnev, M.G. Ramsey, F.P. Netzer, Top. Catal. 94 (2001) 4240.
[40] G.T. Went, S.T. Oyama, A.T. Bell, J. Phys. Chem. 94 (1990) 4240.
[41] H. Miyata, K. Fujii, T. Ono, Y. Kubokawa, T. Ohno, F. Hatayama, J. Chem. Soc., Faraday Trans. 83 (1) (1987) 675.
[42] M. Frank, K. Wolter, N. Magg, M. Heemeier, R. Kühnemuth, M. Bäumer, H.-J. Freund, Surf. Sci. Lett. 492 (2001) 270.
[43] N. Magg, J.B. Giorgi, M.M. Frank, B. Immaraporn, T. Schroeder, M. Bäumer, H.-J. Freund, J. Am. Chem. Soc. 126 (2004) 3616.
[44] G. Herzberg, Molecular Spectra and Molecular Structure, van Nostrand, Princeton, 1950.
[45] G. Pacchioni, Surf. Rev. Lett. 7 (2000) 277.
[46] V. Brázdová, M.V. Ganduglia-Pirovano, J. Sauer, submitted for publication.
[47] M.A. Vuurman, I.E. Wachs, J. Phys. Chem. 96 (1992) 5008.
[48] M.A. Banares, I.E. Wachs, J. Raman Spectrosc. 33 (2002) 359.
[49] A. Christodoulakis, M. Machli, A.A. Lemonidou, S. Boghosian, J. Catal. 222 (2004) 293.
[50] G.G. Cortez, M.A. Banares, J. Catal. 209 (2002) 197.
[51] S.T. Oyama, G.T. Went, K.B. Lewis, A.T. Bell, G.A. Somorjai, J. Phys. Chem. 93 (1989) 6786.
[52] B. Olthof, A. Khodakov, A.T. Bell, E. Iglesia, J. Phys. Chem. B 104 (2000) 1516.
[53] U. Scharf, M. Schraml-Marth, A. Wokaun, A. Baiker, J. Chem. Soc., Faraday Trans. 87 (1991) 3299.